PLD3 gene and processing of APP

Authors:

Pietro Fazzari[1,2,+], Katrien Horre[1,2], Amaia M. Arranz[1,2], Carlo Sala Frigerio[1,2], Takashi Saito[3,4], Takaomi C Saido[3], Bart De Strooper[1,2,5*]

Publication type: Brief Communication Arising

ARISING FROM, C. Cruchaga et al. Nature 505, 550–554 (2014); doi:10.1038/nature12825

(1) VIB Center for the Biology of Disease, Leuven, Belgium
(2) Center for Human Genetics, Leuven Institute for Neurodegenerative Disorders (LIND) University Hospitals Leuven, and University of Leuven, O&N4 Herestraat, Leuven, Belgium
(3) Laboratory for Proteolytic Neuroscience, RIKEN Brain Science Institute, Wako-shi, Saitama, Japan
(4) Japan Science and Technology Agency, Saitama, Japan
(5) UCL Institute of Neurology, Queen Square, London, UK

Pietro Fazzari, Pietro.Fazzari@med.kuleuven.be

Katrien Horre, Katrien.Horre@cme.vib-kuleuven.be

Amaia M. Arranz, amaia.arranz@cme.vib-kuleuven.be

Carlo Sala Frigerio, Carlo.SalaFrigerio@cme.vib-kuleuven.be

Takashi Saito, takasai@brain.riken.jp

Takaomi C Saido, saido@brain.riken.jp

[+] Current affiliation: CBM Severo Ochoa Department of Molecular Neurobiology, CSIC / UAM, Madrid, Spain. Mail: pfazzari@cbm.csic.es

* Correspondence should be addressed to Professor Bart De Strooper:

bart.destrooper@cme.vib-kuleuven.be

VIB Center for the Biology of Disease
KU Leuven,
O&N 4, 6e verd
Campus Gasthuisberg
Herestraat 49, bus 602
3000 LEUVEN, Belgium

Phone: +32 16 37 32 46

Cruchaga *et al*.[1] recently showed that i) variants in the phospholipase D3 (*PLD3*) gene confer increased risk for the development of Alzheimer's disease (AD), ii) PLD3 expression is decreased in sporadic AD patients and iii) the expression of PLD3 inversely correlates with the expression of Amyloid Precursor Protein (APP) and the production of Aβ peptides *in vitro* in cell lines. Altogether, the genetic and functional data led the authors to conclude that PLD3 loss-of-function confers an increased AD risk by affecting APP processing. Here we tested the relevance of Pld3 for APP processing *in vivo* in physiological conditions and in an AD-relevant model: Pld3 deficiency did not affect App metabolism or amyloid plaque burden. PLD3 is however localized in the lysosomal compartment and its loss-of-function alters its morphology, suggesting alternative functions for PLD3 in neurodegeneration.

To test the effect of loss-of-function of PLD3 on brain physiology we acquired the *Pld3*$^{tm1e(EUCOMM)Wtsi}$ mice (*Pld3*^{ko})[2]. These mice carry a trapping cassette with a splicing acceptor followed by a IRES:lacZ knocked-in in the *Pld3* gene (Extended Data Fig. 1a). This insertion abrogates the expression of *Pld3* and results in the expression of the β-galactosidase reporter instead (Extended Data Fig. 1b). Western blot (WB) analysis (not shown) and X-gal staining showed that Pld3 is highly expressed in the pyramidal neurons of cortex and hippocampus; conversely, expression of the β-galactosidase was not detectable in the interneurons of the hippocampus nor in the glial cells of the corpus callosum (Extended Data Fig. 1d, 1d', 1d'' and 1d'''). Morphometric analysis of the gross morphology of *Pld3*-deficient brains did not reveal any major abnormalities as compared to controls (Extended Data Fig. 1e and 1f).

We investigated the effect of genetic deletion of *Pld3* on App proteolysis. mRNA levels of *App* and different candidate genes, including *Adam10*, *Bace1* and the γ-secretase complex subunits, are unchanged in *Pld3*-deficient cortices relative to control brains (Extended Data Fig. 1c). Moreover, WB analysis shows that the expression of App full length (App FL), App C-terminal fragments (App CTF) and the ratio between App CTF and App FL are not affected by *Pld3* deletion in neither the cortex nor the hippocampus (Fig. 1a, b and Extended Data Fig 1g,h). Finally, we assessed the levels of Aβ40 and Aβ42 in control and *Pld3*-deficient mice by performing enzyme-linked immunosorbent assays (ELISA). Significantly, genetic deletion of *Pld3* does not affect endogenous Aβ40 and Aβ42 generation in the cortex and hippocampus of 3-month old adult mice (Fig. 1b and Extended Data Fig. 1h).

To establish the relevance of Pld3 in an AD-relevant model, we crossed *Pld3*^{ko} mice with App knock-in mice (*App*^{ki}) which have a humanized Aβ sequence in the endogenous App gene and contains three clinical relevant mutations to increase amyloidogenesis[3]. The model proposed by Cruchaga et al. predicts that loss of *Pld3* function would increase amyloid burden. Consistent with the experiments above, *Pld3* deletion did not alter the levels of App FL, App CTFs nor the App CTF/App FL ratio (Fig. 1c,d). The levels of Aβ40 and Aβ42 in tris-buffered saline (TBS)-soluble and GuanidineHCl (Gu)–soluble fractions were not increased in *Pld3*^{ko}*;App*^{ki} compared to control mice (Fig. 1d and Extended Data Fig. 1i). Most importantly, *Pld3* deletion did not have any effect on amyloid plaques burden (Fig. 2a,b) further confirming that Pld3 does not affect App metabolism in this AD-relevant mouse model. Future studies will be required to investigate the effect of Pld3 deletion in aged mice or in other AD-models (e.g. tau or ApoE models).

We tried then to replicate the *in vitro* studies of Cruchaga *et al. using* transiently expressing PLD3 wild-type (WT), the catalytically inactive PLD3 K418R (KR)[4] and the AD-

linked PLD3 V232M (VM) variant in HEK293T cells stably expressing human APP-WT. The results of these experiments turned out to be contradictory and highly variable. For instance and consistently with the work of Cruchaga *et al*., we observed a reduction in Aβ levels in cells expressing the PLD3 WT and mutant proteins (Extended Data Fig. 2a). In contrast to Cruchaga *et al*., APP FL were however not significantly affected by PLD3 expression (Extended Data Fig. 2b,c). Unexpectedly, the expression of AD-associated PLD3 VM variant, proposed by Cruchaga *et al*. as loss-of-function allele, also decreased Aβ generation. Notably, the overexpression of PLD3 in these experiments was >50 fold higher than the endogenous expression (not shown). We reasoned that the discrepancies in the results are likely explained by overexpression artefacts e.g. huge overexpression may lead to mislocalization of the protein-of-interest resulting in non-physiological interactions. Therefore, we further investigated the functional relevance of changes in PLD3 expression by utilizing milder overexpression conditions to more closely mimic a physiologically relevant context. We expressed decreasing amounts of PLD3 WT and the KR and VM mutants by Neon® electroporation in HEK293T cells to allow for a more uniform expression of the PLD3 protein (about 20, 5 and 2 fold the endogenous level, Fig. 1u short and long exposures for PLD3). In this experimental paradigm, the expression of PLD3 WT and mutants does not reduce neither Aβ levels (Fig.1t) nor APP expression (Fig. 1u and 1f) confirming that the reported effects of Pld3 on APP reported in Cruchaga et al. are artefacts due to huge overexpression of PLD3.

Several AD-linked genes, that do not directly control APP processing, converge on the regulation of endosomal-autophagic-lysosomal function[5], although the etiological role of endosomal-lysosomal impairment in AD is not completely understood[6,7]. Notably, defects in the endosomal-lysosomal system were found in AD brains[8]. Thus, we investigated the localization of Pld3 in early endosomes (stained with Early Endosome Antigen 1 (EEA1) marker) and in late endosomes and lysosomes (visualized with Lysosomal-associated membrane protein 1 (LAMP-1) marker). Pld3 was not enriched in early endosomes but was mostly localized to LAMP1 positive compartments (Extended Data Fig. 3a-d). Hence, we analysed by electron microscopy (EM) the ultrastucture of lysosomes in *Pld3^{ko}* neurons. Primary and secondary lysosomes of *Pld3* deficient CA1 neurons displayed an increase in density, size and in total area occupied (Extended data Fig. 3e-g). Moreover, several of these secondary lysosomes showed electron-transparent inclusions compatible with lipid droplets (16 out of 73 secondary lysosomes in *Pld3^{ko}* vs 1 out of 22 in control brains). The identification of the precise mechanisms underpinning these alterations is out of the scope of the current study, nonetheless these results show that Pld3 is required to preserve the structure of lysosomes *in vivo*.

In sum, our *in vivo* studies demonstrate that Pld3 is not relevant for App metabolism neither in wild type mice nor in a model of AD pathology. These data challenge the mechanistic model proposed by Cruchaga et al. and suggest a more complex role of PLD3 in the etiology of AD. Our findings that PLD3 protein is localized in and affects the morphology of the lysosomal system indicate that PLD3 may be involved in the pathophysiology of AD by exacerbating the known impairments of endosomal-lysosomal systems[5].

References

1. Cruchaga, C. *et al.* Rare coding variants in the phospholipase D3 gene confer risk for Alzheimer's disease. *Nature* **505,** 550–4 (2014).

2. Skarnes, W. C. *et al.* A conditional knockout resource for the genome-wide study of mouse gene function. *Nature* **474,** 337–342 (2011).

3. Saito, T. *et al.* Single App knock-in mouse models of Alzheimer's disease. *Nat Neurosci* **17,** 661–663 (2014).

4. Osisami, M., Ali, W. & Frohman, M. a. A role for phospholipase D3 in myotube formation. *PLoS One* **7,** (2012).

5. Nixon, R. a. The role of autophagy in neurodegenerative disease. *Nat. Med.* **19,** 983–997 (2013).

6. Boland, B. *et al.* Macroautophagy is not directly involved in the metabolism of amyloid precursor protein. *J. Biol. Chem.* **285,** 37415–37426 (2010).

7. Lee, S., Sato, Y. & Nixon, R. A. Lysosomal Proteolysis Inhibition Selectively Disrupts Axonal Transport of Degradative Organelles and Causes an Alzheimer's-Like Axonal Dystrophy. *J. Neurosci.* **31,** 7817–7830 (2011).

8. Cataldo, a M., Hamilton, D. J., Barnett, J. L., Paskevich, P. a & Nixon, R. a. Properties of the endosomal-lysosomal system in the human central nervous system: disturbances mark most neurons in populations at risk to degenerate in Alzheimer's disease. *J. Neurosci.* **16,** 186–199 (1996).

9. Morishima-Kawashima, M. *et al.* Effect of apolipoprotein E allele epsilon4 on the initial phase of amyloid beta-protein accumulation in the human brain. *Am. J. Pathol.* **157,** 2093–9 (2000).

Authors contribution

PF, conceived the project, planned the experiments, performed the experiments, analysed the results and wrote the manuscript; KH, performed *in vitro* experiments, and performed WB and ELISA analysis *in vitro* and *in vivo* (Fig. 1g-n and Fig. 1q-v); AMA, performed EM experiments and helped to analyse the data; CSF, performed and analysed qPCR experiments (Fig. 1b-c); TS, TCS, previously characterized and provided App knock-in mice; BDS, conceived and supervised the project, wrote the manuscript. All the authors revised the manuscript and helped with comments and feedback.

Acknowledgements.

cDNAs for human PLD3 WT and KR were kindly provided by Prof. Frohman. This work

was supported by the European Research Council (ERC) ERC-2010-AG_268675 to BDS, the Fonds voor Wetenschappelijk Onderzoek (FWO), the KU Leuven and VIB, a Methusalem grant of the KU Leuven/Flemish Government to BDS. BDS is supported by the Bax-Vanluffelen Chair for Alzheimer's Disease and "Opening the Future" of the Leuven Universiteit Fonds (LUF). Confocal microscope equipment was acquired through a Hercules Type 1 AKUL/09/037 to W. Annaert. Mouse experiments were supported by Inframouse (KU Leuven and VIB infrastructure).

Material and methods

HEK293T cells were transfect with TransIT-LT1® (Mirusbio, USA, product nos.MIR2300) or electroporated with Neon® (Invitrogen, Catalog Number MPK5000) according to manufacturer instructions. *Pld3*$^{tm1e(EUCOMM)Wtsi}$ mice (*Pld3*^{ko}) were obtained from The European Mouse Mutant Archive-EMMA. *App*$^{NL-G-F/NL-G-F}$ knock-in mice (*App*^{ki}) that carry the human Aβ sequence with triple Swedish, Arctic and Beyreuther/Iberian mutations were generated as described[3]. Detailed experimental procedures are provided in Supplemental Materials and Methods.

Supplemental material and methods

cDNA for PLD3 VM was generated by site directed mutagenesis and verified by sequencing.

Cell lysates were prepared in STE with 1% Triton X-100. Densitometric quantification of WB were normalized for Actin levels. For the ELISA we collected cell supernatant and measured for Aβ by standard techniques. Data obtained were corrected for the levels of total intracellular protein measured by BCA.

For quantitative PCR, RNA was retrotranscribed to cDNA with oligo dT primers using the SUperScript II Reverse transcriptase kit (Invitrogen). Real-time PCR was carried out using the LightCycler 480 SYBR Green I Master mix (Roche) on a LightCycler LC480 (Roche) instrument.

For β-galactosidase activity brains were perfused with PBS, snap frozen and cut at cryostat. 10 µm sections were fixed for 10 minutes in 0.2 % glutaraldehyde, rinsed and incubated in X-Gal staining solution according to standard procedure.

Samples from control and *Pld3*^{ko} mice were lysate in 0.4% Diethylamine, 50 mM NaCl, 50 mM Tris-HCl buffer with EDTA free protease inhibitors and processed for WB or ELISA. WB densitometry and ELISA were normalized as for cells lysates above. Brains from control and *Pld3*^{ko}*;App*^{ki} mice were perfused in PBS. Next, half brain was postfixed in 4% PFA, rinsed, cut at 100 µm at the vibratome and processed for thioflavin staining; the other half was homogenised in tissue protein extraction reagent (Pierce) with protease inhibitors. Extraction of TBS- and Gu-soluble Aβ was performed as described[9].

Thioflavin staining was performed according to standard technique, for confocal imaging we used Olympus FV1000 IX2 Inverted Confocal microscope with 20x UPlanSapo. Images were automatically thresholded and quantified with ImageJ.

Colabelling of PLD3 in HEK293 cells with EEA1 and LAMP1 was done with the antibodies anti-PLD3 (Sigma, #HPA012800; dilution 1/200), anti-EEA1 (BD, #610456; 1/500) and anti-LAMP1 (Santa cruz, #sc-19992; 1/500) according to standard IF techniques. Samples were fixed in PFA 4% for 10 minutes. Pictures were taken with an Olympus FV1000 IX2 Inverted Confocal microscope with 60x UPlanSapo. Generation of PDM image and quantification of Pearson's and Mander's coefficients was performed using the ImageJ Plug-in "Intensity Correlation Analysis".

For EM analysis, *Pld3*^{ko} mice and control littermates were perfused at 1 month with 2.5% glutaraldehyde, 2% paraformaldehyde in 0.1 M cacodylate buffer. 300 µm coronal brain sections were cut on a vibratome and rectangular pieces of tissue comprising the CA1 region were dissected. Briefly, the tissue was post-fixed with 1% OsO4, 1.5% K4Fe(CN)6 in 0.1 M cacodylate buffer, rinsed, stained with 3% uranyl acetate and dehydrated in graded

ethanols and propyleneoxide, followed by embedding in EMbed812. 70 nm ultrathin sections were mounted on copper grids and imaged at 3000x using a JEM-1400 transmission electron microscope (Jeol).

Figure legends

Figure 1

a, WB of lysates from control and *Pld3*^{ko} show APP FL, APP CTF and Pld3 expression in cortex at 3 months.

b, Densitometry of WB and ELISA quantification Aβ40 and Aβ42 levels in cortex from *Pld3*^{ko} mice relative to control mice. n>7 control and n=10 *Pld3*^{ko} mice. Graphs show mean ± SEM.

c, WB of lysates from control and *Pld3*^{ko}*;App*^{ki} show APP FL, APP CTF and *Pld3* expression in cortex at 4 months.

d, Densitometry of WB and ELISA of TBS- Aβ40 and Aβ42. Graphs show mean ± SEM. n=8 for both Ctrl and Pld3^{ko};App^{ki}.

Figure 2

a, Confocal images of thioflavin stained cortices from control and *Pld3*^{ko}*;App*^{ki} mice. Scale bar 50 μm.

b, Quantification of amyloid plaques burden as percentage of area occupied by the plaques. Graphs show mean ± SEM. n=8 for both Ctrl and *Pld3*^{ko}*;App*^{ki}.

Extended Data Figure legends

Extended Data 1

a, Schema of the *Pld3* targeted inactivation and LacZ-tagging strategy in *Pld3*^{ko} mice. The trapping cassette with a splicing acceptor followed by a IRES:lacZ knocked-in was inserted between exon 9 and 10. Coloured bars indicate the primer binding sites of qPCRs (shown in **b**). SA, splicing acceptor; IRES, internal ribosome entry site; neo, neomycine cassette.

b, Validation of *Pld3* inactivation by qPCR. The expression of exons 7-8 is strongly reduced, while exons 9-10 are not detectable (nd) in *Pld3*^{KO} mice which express LacZ instead at 1 month (e9-LacZ). Expression levels are plotted relative to respective reference. nd, expression value < 0.005. n=6 for Ctrl and Pld3^{ko} mice; Graphs represent the mean ± SD; ***P<0.001. T test.

c, qPCR expression analysis of mRNA of *App* and of genes involved in its processing in *Pld3*^{ko} relative to control mice at 1 month. n=6 for WT and *Pld3*^{ko} mice; Graphs represent the mean ± SD.

d, X-gal staining of *Pld3*^{het} brain show the expression of *Pld3* in neurons at 1 month. Fast red is used as counterstaining. Cx, cortex; cc, corpus callosum; Hip, hippocampus; so, stratum oriens; sp, stratum pyramidalis; sr, stratum radiatum; DG, dentate gyrus. Scale bar 500 µm. **l'**,**l''** and **l'''** show insets from **l** in sp, so and cc respectively. Scale bar 20 µm. **l'**, X-gal staining in CA1 pyramidal layer of the hippocampus. **l''**, **l'''**, β-galactosidase activity is not detectable in interneurons of the hippocampus (full arrowheads in **l''**) nor in the glia cells of the corpus callosum (empty arrowheads in **l'''**).

e, Dorsal, lateral; and central view of representative brains from control and *Pld3*^{ko} mice at 3 months. w, width; l, length; h, height; t, thickness.

f, Morphometric quantification of **e**. Graphs show mean ± SD. n=2 Ctrl and n=3 *Pld3*^{ko} Scale bar 2 mm.

g, Representative WB of lysates from control and *Pld3*^{ko} show APP FL, APP CTF and Pld3 expression in hippocampus at 3 months.

h, Densitometric analysis of WB and ELISA quantification Aβ40 and Aβ42 levels in hippocampus from *Pld3*^{ko} mice relative to control mice. n>7 control and n=10 *Pld3*^{ko} mice from three litters. Graphs show mean ± SEM.

i, ELISA of GU-soluble Aβ40 and Aβ42. Graphs show mean ± SEM. n=8 for both Ctrl and Pld3^{ko};App^{ki}; ** P<0.01, two-way ANOVA.

Extended Data 2

a, Enzyme-linked immunosorbent assay (ELISA) shows the levels of Aβ40 and Aβ42 in the supernatant of HEK293T transfected with TransIT-LT1 to express either GFP as control or PLD3 WT, PLD3 KR, and PLD3 VM. Aβ levels are expressed relative to control. Graph shows mean ± SEM. n=6 out of 2 experiments. ***, P<0.001. Two-way ANOVA.

b, Representative WBs show APP FL, APP CTF and PLD3 in lysates from HEK293T cells from the experiment in **q**.

c, Densitometric analysis of WBs from the experiment in **q**,**r**. Graphs shows mean ± SEM. n=6 out of 2 experiments. *, P<0.05. Two-way ANOVA.

d, Levels of Aβ40 and Aβ42 in the supernatant of HEK293 cells electroporated with 2.5, 0.75, and 0.25 μgr of PLD3 WT, PLD3 KR, and PLD3 VM relative to GFP electroporated control cells. Graphs shows mean ± SEM. n=6 out of 3 experiments. *, P<0.05. Two-way ANOVA.

e, Representative WBs show APP FL, APP CTF and PLD3 in lysates from **d**. For PLD3 short and long exposures of the same blot are shown.

f, Densitometry of WBs from **e**. Levels are relative to control. Graphs shows mean ± SEM. n=6 out of 3 experiments.

Extended Data 3

a, Confocal images show that PLD3 does not colocalize with EEA1 in early endosomes. The inset shows area magnified in the right panels. Product of the difference of the mean (PDM) image illustrates the negative correlation of PLD3 and EEA1 (light blue arrowheads). The right bar shows colour codes for PDM values (negative in blue and positive in orange). Scale bars 5 μm.

b, Pearson coefficients for EEA1/PLD3 (n=5) and LAMP1/PLD3 (n=7). Graph shows Means ± SEM.

c, PLD3 is mostly localized in LAMP1 positive late endosomes/lysosomes. The inset shows area magnified in the right panels. PDM image shows the positive correlation of PLD3 and LAMP1 staining (yellow arrowheads). Scale bars 5 μm. Colour scales indicate PDM values.

d, Mander's coefficients for LAMP1 and PLD3 co-labelling. Graph shows Means ± SEM, n=7.

e, Representative EM pictures of primary and secondary lysosomes (white and black arrowheads respectively) from control and Pld3 deficient neurons. The arrow indicates electron-transparent inclusion in a secondary lysosome. Scale bars: 500 nm.

f, Density, size and area occupied by primary lysosomes. Graph shows Means ± SEM. For density and area: Ctrl, n = 50 fields out of 2 brains; *Pld3*^{ko}, n = 84 out of 3 brains. For density: *p<0.05, Mann Whitney test. For area: ***p<0.001, T test. For size: Ctrl: n=91; Pld3^{ko}, n=208; ***p<0.001, T test.

g, Density, size and area occupied by secondary lysosomes. Graph shows Means ± SEM. For density and area: Ctrl, n = 50 fields out of two brains; *Pld3*^{ko}, n = 84 out of 3 brains. For density: *p<0.05, Mann Whitney test. For area: ***p<0.001, T test. For size: Ctrl: n=22; *Pld3*^{ko}, n=73; *p<0.05, T test.

Figure 1

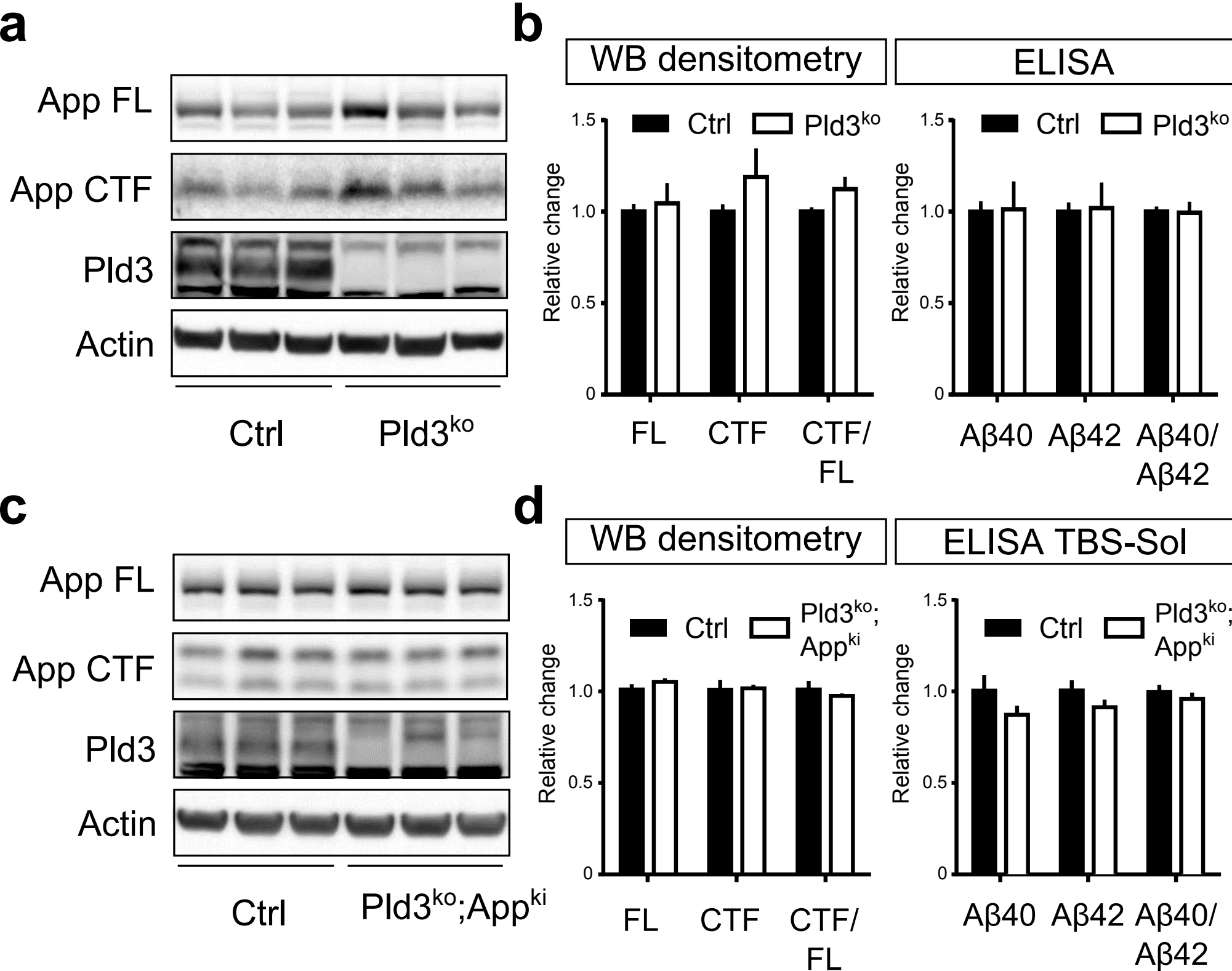
a
App FL
App CTF
Pld3
Actin
Ctrl
Pld3ko
b
WB densitometry
ELISA
Ctrl
Pld3ko
Relative change
1.5
1.0
0.5
0
FL
CTF
CTF/ FL
Aβ40
Aβ42
Aβ40/ Aβ42
c
App FL
App CTF
Pld3
Actin
Ctrl
Pld3ko;Appki
d
WB densitometry
ELISA TBS-Sol
Ctrl
Pld3ko; Appki
Relative change
1.5
1.0
0.5
0
FL
CTF
CTF/ FL
Aβ40
Aβ42
Aβ40/ Aβ42

Figure 2

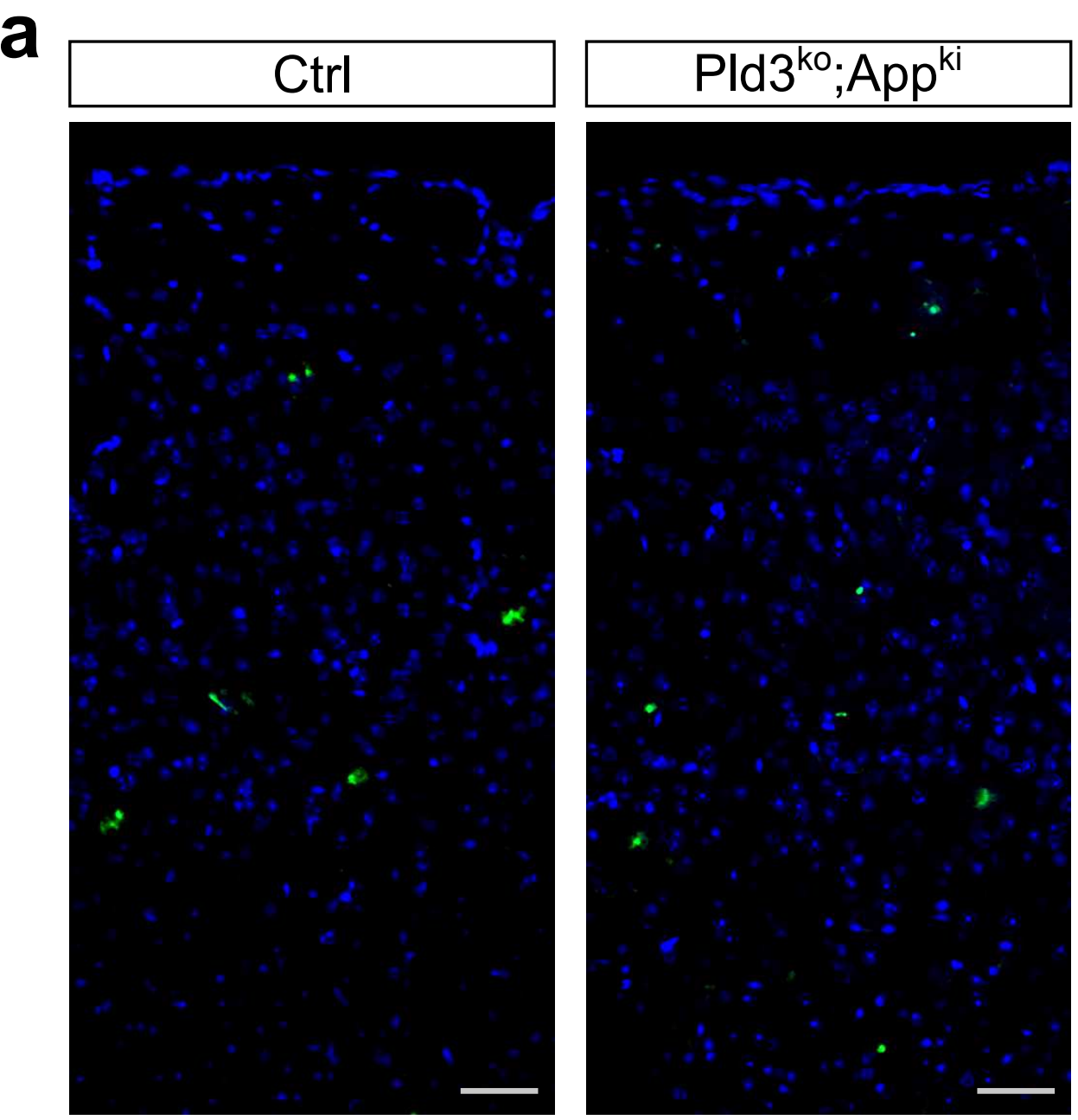
a
Ctrl
Pld3ko;Appki

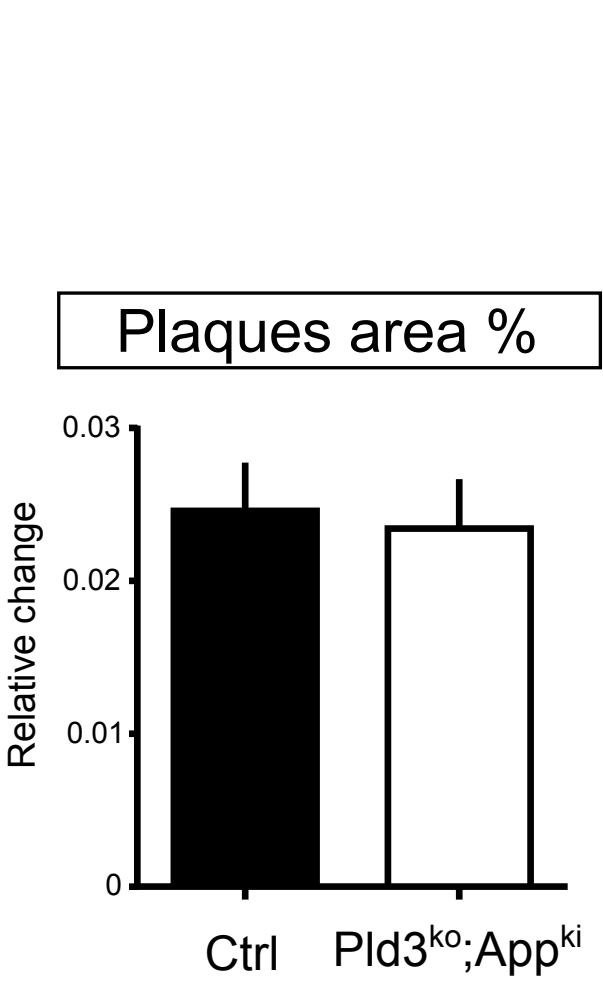
b
Plaques area %
Relative change
0.03
0.02
0.01
0
Ctrl
Pld3ko;Appki